JGP Journal of General Physiology

RESEARCH ARTICLE

Propofol inhibits the voltage-gated sodium channel NaChBac at multiple sites

Yali Wang[1], Elaine Yang[2], Marta M. Wells[1,3], Vasyl Bondarenko[1], Kellie Woll[4], Vincenzo Carnevale[5], Daniele Granata[5], Michael L. Klein[5], Roderic G. Eckenhoff[4], William P. Dailey[6], Manuel Covarrubias[2], Pei Tang[1,3,7], and Yan Xu[1,7,8,9]

Voltage-gated sodium (Na_V) channels are important targets of general anesthetics, including the intravenous anesthetic propofol. Electrophysiology studies on the prokaryotic Na_V channel NaChBac have demonstrated that propofol promotes channel activation and accelerates activation-coupled inactivation, but the molecular mechanisms of these effects are unclear. Here, guided by computational docking and molecular dynamics simulations, we predict several propofol-binding sites in NaChBac. We then strategically place small fluorinated probes at these putative binding sites and experimentally quantify the interaction strengths with a fluorinated propofol analogue, 4-fluoropropofol. In vitro and in vivo measurements show that 4-fluoropropofol and propofol have similar effects on NaChBac function and nearly identical anesthetizing effects on tadpole mobility. Using quantitative analysis by ^{19}F-NMR saturation transfer difference spectroscopy, we reveal strong intermolecular cross-relaxation rate constants between 4-fluoropropofol and four different regions of NaChBac, including the activation gate and selectivity filter in the pore, the voltage sensing domain, and the S4–S5 linker. Unlike volatile anesthetics, 4-fluoropropofol does not bind to the extracellular interface of the pore domain. Collectively, our results show that propofol inhibits NaChBac at multiple sites, likely with distinct modes of action. This study provides a molecular basis for understanding the net inhibitory action of propofol on Na_V channels.

Introduction

Excitable cells such as neurons and myocardia communicate with each other by alternating electrical and chemical signals. The electric impulses travel along the cell surface by means of depolarization and repolarization involving the flow of Na^+ and K^+ ions in opposite directions across the cell membrane. The voltage-gated sodium (Na_V) channels, which typically conduct the Na^+ current inward, are responsible for controlling the initiation and propagation of action potentials. Na_V channels are involved in a variety of physiological processes, including skeletal muscle contraction, heart rhythm, and neurotransmission. Accordingly, drugs that affect Na_V channel function include anticonvulsants, antiarrhythmics, and antiepileptics, as well as local anesthetics (Amarouch and Abriel, 2015; Habib et al., 2015; Lin and Baines, 2015; Jeevaratnam et al., 2016).

Unlike local anesthetics, it has been widely believed that general anesthetics primarily exert their action by targeting postsynaptic ligand-gated ion channels (Eckenhoff and Johansson, 1997; Tang and Xu, 2002; Liu et al., 2009; Chen et al., 2010; Pan et al., 2012; Mowrey et al., 2013; Tillman et al., 2013; Bondarenko et al., 2014). However, recent experimental evidence suggests that Na_V channels also play a critical role in the disruption of synaptic transmission by general anesthetics. Several functional studies with heterologously expressed eukaryotic Na_V channels (OuYang and Hemmings, 2007; Purtell et al., 2015) and their bacterial counterparts (Hemmings et al., 2005; Barber et al., 2014; Kinde et al., 2016; Sand et al., 2017) have demonstrated that clinically relevant concentrations of general anesthetics can inhibit the function of Na_V channels. Although local anesthetics are known to block the Na_V channel pore and stabilize the inactivated state (Goldschen-Ohm and Chanda, 2014), the modes of action of general anesthetics on Na_V channels remain elusive.

General anesthetics bind to their protein targets, including Na_V channels, with relatively low affinity (high micromolar to low millimolar) and high exchange rates. These low-affinity

[1]Department of Anesthesiology, University of Pittsburgh School of Medicine, Pittsburgh, PA; [2]Department of Neuroscience and Vickie and Jack Farber Institute for Neuroscience, Sidney Kimmel Medical College and Jefferson College of Biomedical Sciences, Thomas Jefferson University, Philadelphia, PA; [3]Department of Computational and Systems Biology, University of Pittsburgh School of Medicine, Pittsburgh, PA; [4]Department of Anesthesiology and Critical Care, University of Pennsylvania, Philadelphia, PA; [5]Institute for Computational Molecular Science, College of Science and Technology, Temple University, Philadelphia, PA; [6]Department of Chemistry, University of Pennsylvania, Philadelphia, PA; [7]Department of Pharmacology and Chemical Biology, University of Pittsburgh School of Medicine, Pittsburgh, PA; [8]Department of Structural Biology, University of Pittsburgh School of Medicine, Pittsburgh, PA; [9]Department of Physics and Astronomy, University of Pittsburgh, Pittsburgh, PA.

Correspondence to Yan Xu: xuy@anes.upmc.edu.

binding interactions are often difficult to characterize with traditional biophysical methods because of the transient nature of the anesthetic–target complex. The conventional association or disassociation constant (K_a or K_d) measures the apparent or time-averaged drug–protein interactions with little binding-site information. In contrast, saturation transfer difference (STD) NMR spectroscopy is particularly well suited for quantifying anesthetic binding to proteins as it is a ligand-based detection method that can be used to probe low-affinity interactions (K_d in the micromolar to millimolar range) via selective magnetization transfer from a macromolecule to a small ligand bound under fast chemical exchange conditions (Mayer and Meyer, 1999). The rate of saturation transfer depends on the mobility of the protein and the ligand, the lifetime of the complex, and ligand-binding geometry (Streiff et al., 2004; Angulo et al., 2010; Venkitakrishnan et al., 2012). Accordingly, previous studies have shown that the STD cross-relaxation rate constant (initial growth rate of the STD signal) is a measure of ligand affinity and can be used to determine K_d when measured across a range of ligand concentrations (Angulo et al., 2010; Künze et al., 2014, 2016; Zhang et al., 2017; Chan et al., 2018). In particular, ^{19}F STD NMR experiments are advantageous compared with standard ^{1}H STD NMR because ^{19}F-NMR background signal is absent in protein, lipids, and water. Thus, ^{19}F spectra allow for not only differentiation of signals that are difficult to distinguish in ^{1}H spectra (Danielson and Falke, 1996; Lepre et al., 2004; Wagstaff et al., 2013) but also identification of drug-binding site by selective ^{19}F probe placement in the protein. In addition, the gyromagnetic ratio of ^{19}F is close to that of ^{1}H ($\gamma_F/\gamma_H \sim 0.94$) (Lepre et al., 2004); the distance limit of detection for ^{19}F STD NMR measurements is similar to that of standard ^{1}H STD NMR ($r < 10$ Å) (Jayalakshmi and Rama Krishna, 2002, 2004).

The bacterial sodium channel from *Bacillus halodurans* (NaChBac) is a structural homologue of eukaryotic Na_V channels (Ren et al., 2001) that provides a convenient model to study the anesthetic interactions with Na_V channels because NaChBac is easily produced in large quantities and with high purity. Several studies have shown that NaChBac, other bacterian Na_V channels, and eukaryotic Na_V channels are dose-dependently inhibited by the intravenous general anesthetic propofol (Frenkel and Urban, 1991; Rehberg and Duch, 1999; Haeseler and Leuwer, 2003; Ouyang et al., 2003; Haeseler et al., 2008; Stoetzer et al., 2016; Yang et al., in this issue). Although eukaryotic and prokaryotic Na_V channels are evolutionarily distinct—with the former being a single amino acid chain folded into a pseudotetrameric channel and the latter being a homotetrameric assembly of four identical subunits—these channels nevertheless share many similar structural features. Both eukaryotic and prokaryotic Na_V channels consist of four voltage-sensing domains (VSDs), each composed of S1–S4 helices, and a pore domain (PD) composed of S5–S6 helices and a P-loop arranged in a tetrameric ring to form an ion-conducting channel. A helical S4–S5 linker, situated at the cytoplasmic moiety of the membrane bilayer, connects the VSD to the PD.

In previous studies, we demonstrated that the volatile general anesthetics isoflurane and sevoflurane dose-dependently inhibit NaChBac (Barber et al., 2014; Kinde et al., 2016). Using site-directed labeling with small fluorinated probes, we further quantified the specific binding of isoflurane to various regions in NaChBac using ^{19}F STD NMR (Kinde et al., 2016). In the current study, in silico predictions of propofol-binding sites were used to guide similar site-directed labeling to five different regions of NaChBac. Unlike isoflurane, propofol does not naturally contain the fluorine atoms required for ^{19}F STD NMR, so a fluorinated propofol analogue (4-fluoropropofol) was synthesized. In vivo measurements of anesthesia were conducted to ensure that the physiological effects of the analogue were comparable to that of propofol, and in vitro electrophysiology experiments were performed to confirm that the mutations required for site-directed labeling in NaChBac did not obstruct channel gating. Residue-specific binding was quantified by using ^{19}F STD NMR, and the results indicate that propofol binds to multiple regions of NaChBac, including a site in the VSD, a pocket near the S4–S5 linker, and within the PD.

Materials and methods

Molecular modeling

No experimental structure is currently available for NaChBac. A structural model of NaChBac was obtained previously (Barber et al., 2012) based on the crystal structure of a prokaryotic Na_V channel from *Arcobacter butzleri* (NavAb) in a putative closed-pore conformation with all four VSDs partially activated (PDB accession no. 3RVY; Payandeh et al., 2011). Four additional structural models of NaChBac in a variety of putative functional states were obtained by using Modeller 9.17 (Webb and Sali, 2014a,b) based on experimental crystal structures of prokaryotic Na_V channels from *Magnetococcus marinus* (NavMs; PDB accession no. 5HVX; Sula et al., 2017), *Rickettsiales* sp. *HIMB114* (NavRh; PDB accession no. 4DXW; Zhang et al., 2012), and NavAb (PDB accession nos. 5VB2 and 5VB8; Lenaeus et al., 2017). For each crystal structure, 25 independent NaChBac models were generated. The structure with the lowest discrete optimized potential energy was selected for subsequent docking calculations.

Molecular docking

AutoDock version 4.2.6 (Morris et al., 2009) was used for all docking calculations. Docking grids with 0.375-Å spacing were generated to cover the entire transmembrane domain of each protein structure so that all potential binding sites were considered equally. Both propofol and 4-fluoropropofol were docked separately to all five NaChBac structural models as well as each of the original template Na_V channel structures by using a Lamarckian genetic algorithm with a population size of 1,000, a maximum of 27,000 generations, and a maximum of 25 million energy evaluations. A total of 500 independent docking calculations were clustered by using an RMSD cutoff of 2 Å.

MD simulations

The final frame from previous MD simulations of NaChBac embedded in a fully hydrated 1-palmitoyl-2-oleoyl-sn-glycero-3-phosphocholine (POPC) lipid bilayer (Barber et al., 2012) was used as the initial coordinates to simulate flooding NaChBac with propofol. The flooding simulation was performed by using

NAMD2.10 (Phillips et al., 2005). The simulation system contained a total of ~122,000 atoms, including a NaChBac tetramer, 434 lipid molecules (POPC), 25,310 water molecules, 236 ions (Cl^- and Na^+), and 145 propofol molecules. Thus, the water-to-propofol ratio was 174.6, equivalent to an initial aqueous concentration of 0.32 M. Initially, all propofol molecules were randomly distributed in the aqueous phase, and two Na^+ ions were placed in the channel selectivity filter, in agreement with a previous computational study of NavAb showing double occupancy of the filter by Na^+ ions (Carnevale et al., 2011). All charged amino acids were fully ionized at pH 7. The system was equilibrated through three consecutive stages of 500 ps each, in which position restraints on different groups were progressively released. The CHARMM36 force field was used for the phospholipids and CHARMM27 for the protein (Lee et al., 2016). A united-atom representation was adopted for the acyl chains of the POPC lipid molecules (Hénin et al., 2008). Propofol parameters were obtained from the literature (LeBard et al., 2012). Periodic boundary conditions were used, and the electrostatic potential was evaluated by using the particle mesh Ewald method. The lengths of all bonds containing hydrogen were constrained with the SHAKE/RATTLE algorithm. The system was maintained at a temperature of 300°K and pressure of 1 atm by using the Langevin thermostat and barostat methods as implemented in NAMD2.10. The reversible reference system propagation algorithm (rRESPA) multiple time step method was used, with a high-frequency time step of 2 fs and a low-frequency time step of 4 fs. A trajectory of ~1 µs was collected for subsequent analysis.

Site-directed ^{19}F labeling and NMR sample preparation

Single cysteine mutations of NaChBac were prepared by using the same procedures as detailed previously (Kinde et al., 2016). In brief, the QuickChange lightning mutagenesis kit (Agilent) was used to mutate the selected residue to cysteine. The mutated NaChBac was expressed in lysogeny broth at 18°C, purified by using a 5-ml Ni column, and eluted with a buffer solution containing 50 mM Tris, 500 mM NaCl, 500 mM imidazole, and 0.1% n-dodecyl-β-D-maltoside (DDM). Site-directed ^{19}F labeling was achieved by covalent attachment of 3-bromo-1,1,1-trifluoroacetone (BTFA) to individual cysteine residues. BTFA in 50-fold excess was added to purified NaChBac mutants and incubated at 4°C overnight. After the labeling reaction was completed, the ^{19}F-labeled NaChBac in the tetrameric form was purified and separated from the free BTFA by using size-exclusion chromatography (Superdex 75 10/300 GL column; GE Healthcare). The protein samples were further concentrated to 100 µM for NMR measurements. The mutation sites can be grouped into five regions (see Results): (1) the apex of the VSD, including N36C and V40C in the S1 helix immediately above the hydrophobic constriction site; (2) the hinge region of the S4–S5 linker, including S129C and L150C; (3) the selectivity filter region, including T189C at the base of the selectivity filter; (4) the pore region, including I223C in the middle of the central cavity and F227C at the activation gate; and (5) the extracellular interface, including S208C at the hinge of the P2 and S6 helices.

To measure cross-relaxation rate constants between propofol and the fluorinated NaChBac mutants by using ^{19}F STD experiments, we used a fluorinated propofol analogue, 4-fluoro-2,6-diisopropylphenol (or 4-fluoropropofol). In a typical NMR sample, 4-fluoropropofol was titrated into the protein samples in a solution of 1–2% DDM, 50 mM Tris at pH 7.7, 100 mM NaCl, 5% D_2O for deuterium locking, and a final concentration of ~200 µM.

NMR data acquisition and analysis

All NMR experiments were performed on a Bruker Biospin Avance 600 spectrometer, equipped with a ^{19}F cryoprobe and operated at a Larmor frequency of 564.68 MHz for ^{19}F resonance. To maintain protein sample stability, the NMR sample temperature was controlled at 10°C. The STD NMR spectra were acquired by collecting alternating on-resonance and off-resonance ^{19}F spectra with saturation irradiations at –83.8 and –45.00 ppm, respectively. Saturation was achieved by a train of Gaussian cascade (Q3.1000)-shaped pulses of 3 ms and an interpulse delay of 3 ms. Intermolecular ^{19}F STD build-up from the protein resonance to the ligand resonance was determined by using saturation times of 0.05, 0.2, 0.5, 1.0, 2.0, and 4.0 s in a randomized order. The intensities and corresponding errors of 4-fluoropropofol ^{19}F spectra were analyzed by using MestRenova v8.1.4 and TopSpin3.5. The STD data were fit to the following mono-exponential function and analyzed by using Prism 6:

$$STD = STD_{\max}(1 - e^{-k_{sat}t}), \quad (1)$$

where

$$STD\% = \frac{I_{off} - I_{on}}{I_{off}} \times 100, \quad (2)$$

t is saturation time, and I_{on} and I_{off} are 4-fluoropropofol peak intensities with on- and off-resonance saturation of the labeled protein peak, respectively. STD_{max} is the maximum (plateaued) STD, and k_{sat} is the observed saturation rate constant. The cross-relaxation rate constant (σ), which is a direct measure of ligand-protein interaction strength, can be expressed as

$$\sigma = STD_{\max} \times k_{sat}. \quad (3)$$

Electrophysiology

The procedures for preparing materials, performing electrophysiology, and data analysis are detailed previously (Yang et al., 2018b). To generate NaChBac mutants, point mutations were introduced into the WT plasmid by using the QuickChange site-directed mutagenesis method (Agilent). HEK-293 cells were transiently transfected with cDNA by using Lipofectamine 2000 transfection reagent (Invitrogen) and seeded onto 12-mm circular glass coverslips (Fisher Scientific) 24 h before patch-clamp recording. Standard protocols were followed for growth and maintenance of cells in culture.

Voltage-dependent activation was assessed with Na^+ currents evoked by 700-ms depolarizing steps (from –100 to +60 mV, ΔV = 10 mV). The holding potential (V_{hold}) for NaChBac WT, V40C, T189C, and F227C was –120 mV; for NaChBac S129C, V_{hold} was –160 mV. Prepulse inactivation in NaChBac WT, V40C, T189C, and F227C was assessed with a two-pulse protocol: (1) a 2-s conditioning pulse (–120 mV to –10 mV, ΔV = 10 mV), followed immediately by (2) a 50-ms test pulse to +10 mV; V_{hold} was –120 mV. In

NaChBac S129C, the conditioning pulse varied from −140 to −20 mV, ΔV = 10 mV; and V_{hold} was −160 mV. All electrophysiology data are reported as mean ± SEM from *n* separate experiments.

Hypnotic activity in albino *Xenopus laevis* tadpoles

In vivo anesthetizing effects were measured for 4-fluoropropofol and propofol in albino *X. laevis* tadpoles (stages 45–47) as described previously (Hall et al., 2010; Woll et al., 2015). All animal care and experimental procedures involving *X. laevis* tadpoles were performed according to a protocol approved by the Institutional Animal Care and Use Committee of the University of Pennsylvania. In brief, tadpoles were incubated for 30 min in Petri dishes (10 tadpoles per dish) with varying concentrations of 4-fluoropropofol or propofol dissolved in pond water, containing <0.01% DMSO as vehicle. Hypnosis, or immobility, was determined by the percentage of tadpoles that did not demonstrate spontaneous movement in a 30-s evaluation period at the end of the 30-min incubation. After the anesthetic exposures, the tadpoles were transferred to fresh pond water and observed overnight for signs of toxicity. The water temperature was maintained at 21–22°C throughout the experiments. Values are represented as the mean ± SEM for three replicates. Data were fit to the following sigmoidal dose response curve with variable Hill slope:

$$Y = bottom + \frac{top - bottom}{1 + 10^{(logEC_{50} - X) \times HillSlope}}, \quad (4)$$

where X is the logarithm of the concentrations of propofol or 4-fluoropropofol.

Online supplemental material

Fig. S1 shows changes in NaChBac activation and inactivation gating parameters induced by 4-fluoropropofol. Table S1 shows the predicted propofol binding sites identified by molecular docking on template Na_V channel crystal structures. Fig. S2 shows the effects of single-cysteine mutations on the function of NaChBac. Fig. S3 shows the effects of 4-fluoropropofol on NaChBac mutant gating and kinetics. Fig. S4 shows stack plots of ^{19}F STD NMR spectra between 4-fluoropropofol and NaChBac.

Results

4-Fluoropropofol as a surrogate for propofol

Because propofol does not naturally contain any fluorine atoms, a fluorinated analogue was needed to measure the strength of propofol interactions with ^{19}F STD NMR. We synthesized 4-fluoropropofol following a procedure described in the literature (Yuan et al., 2017) and determined the anesthetizing concentrations of propofol and 4-fluoropropofol in vivo by assessing immobility in tadpoles. The percentage of immobilized tadpoles from three separate trials with 10 tadpoles per drug per trial is plotted in Fig. 1 as a function of drug concentration for propofol or 4-fluoropropofol. The EC_{50} values, determined from the nonlinear fitting to the dose–response curves (Eq. 2), are given as mean (95% confidence interval): propofol, 0.89 (0.82–0.96) μM and 4-fluoropropofol, 0.84 (0.73–0.97) μM. Hill slopes are 3.21 ± 0.36 and 2.73 ± 0.49 for propofol and 4-fluoropropofol, respectively. The two-tailed Student's *t* test shows no significant

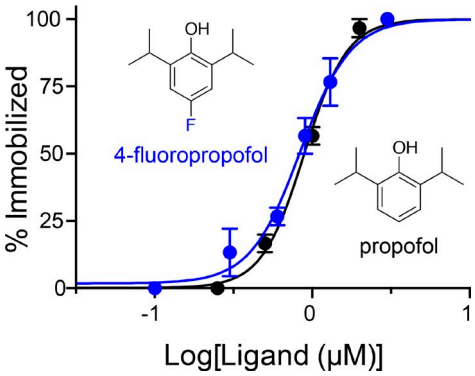

Figure 1. **In vivo anesthetizing concentrations of propofol and 4-fluoropropofol in albino *X. laevis* tadpoles are identical.** The percentage of immobilized tadpoles is plotted as a function of propofol and 4-fluoropropofol concentrations. The solid lines are best fit to the data by using Eq. 4. Error bars show the SEMs from three independent measurements with 10 tadpoles per measurement at each drug concentration.

difference between the anesthetizing potencies of propofol and 4-fluoropropofol.

In addition to the in vivo effects, we also evaluated the in vitro functional relevance of using 4-fluoropropofol to probe propofol action through electrophysiological measurements of NaChBac modulation by 4-fluoropropofol. Fig. 2 summarizes paired electrophysiology measurements in the absence and presence of 4-fluoropropofol. Like propofol, 4 μM 4-fluoropropofol significantly reduced the time constant of inactivation (Fig. 2, A–C) and induced parallel hyperpolarizing shifts of both the G-V (Fig. 2 D, left) and prepulse inactivation curves (Fig. 2 E, left). These shifts corresponded to changes in the midpoint ($\Delta V_{1/2}$) of activation and inactivation of −14.11 ± 1.87 mV and −10.96 ± 0.80 mV, respectively, closely matching the experimental values for propofol as detailed in the companion paper (Yang et al., 2018a).

To evaluate lower affinity interactions, we also examined the functional effects of 4-fluoropropofol at a 10-fold higher (but still clinically relevant) concentration (Khan et al., 2014). At 40 μM, 4-fluoropropofol induced a dramatic acceleration of the current decay (Fig. 2, B and C) and inhibited the peak current by 55% as determined by the average of the paired ratios (Fig. S1 A). This concentration of 4-fluoropropofol also changed the slope of the activation curve, giving some indication of hyperpolarization, but the $V_{1/2}$ of activation did not change significantly (Fig. 2 D, right; and Fig. S1 A). It also strongly hyperpolarized the prepulse inactivation curve, corresponding to a $\Delta V_{1/2}$ of inactivation of −49.87 ± 5.95 mV, and reduced the associated effective gating charge (Fig. 2 E, right; and Fig. S1 B). At higher concentrations, 4-fluoropropofol might inhibit NaChBac by pore blockade and stabilization of the inactivated state, in addition to the gating acceleration effects as seen at lower concentrations (see Discussion). The combined results of the in vitro and in vivo measurements validate the physiological relevance of using 4-fluoropropofol as a fluorinated surrogate of propofol in binding analyses.

Multiple predicted propofol binding sites in NaChBac

As a general anesthetic with relatively low affinity for its protein targets, propofol likely binds to multiple distinct sites in NaChBac

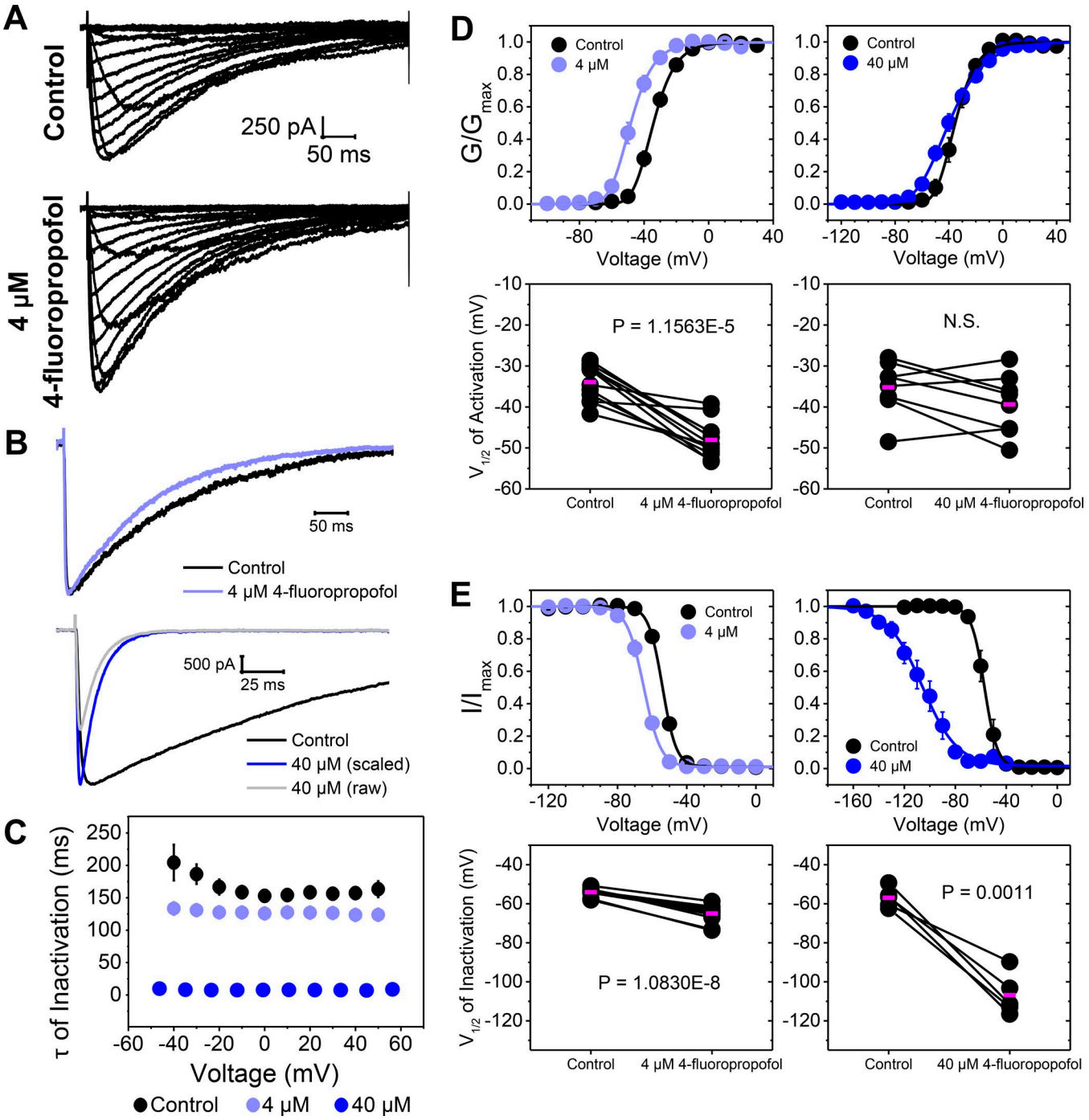

Figure 2. **4-Fluoropropofol modulates voltage-dependent activation and inactivation of NaChBac. (A)** Representative paired current families in the absence (control) and presence of 4 μM 4-fluoropropofol. **(B)** Paired currents at +20 mV. The 4-μM 4-fluoropropofol trace is shown scaled to its respective control I_{peak}. The 40-μM 4-fluoropropofol trace is shown both as a raw current and scaled to its respective control I_{peak}. **(C)** Time constants of inactivation (τ) versus voltage of control (n = 20) and 4-fluoropropofol at 4 and 40 μM (n = 8–12). 4-Fluoropropofol reduced $\tau_{Inactivation}$ at both concentrations and all voltages ($P < 0.0001$, paired t test). **(D and E)** Normalized G-V (D) and prepulse (E) inactivation curves of control and 4-fluoropropofol at the indicated concentrations (n = 5–12). Corresponding midpoints ($V_{1/2}$) of activation and inactivation are shown below the corresponding curves. Means are indicated in magenta. Data are reported as mean ± SEM from n independent measurements.

to produce its net inhibitory effects. To broadly examine all potential propofol-binding sites, we used two complementary computational techniques, molecular docking and MD simulations, as a preliminary screen to guide further experimental quantification. In the molecular docking calculations, both propofol and 4-fluoropropofol were screened on five structural models of NaChBac in a variety of putative functional states. Four distinct binding sites were observed with occupancies ≥10% for either propofol or 4-fluoropropofol (Fig. 3 A and Table 1). Both compounds bound to each of these four sites with similar occupan-

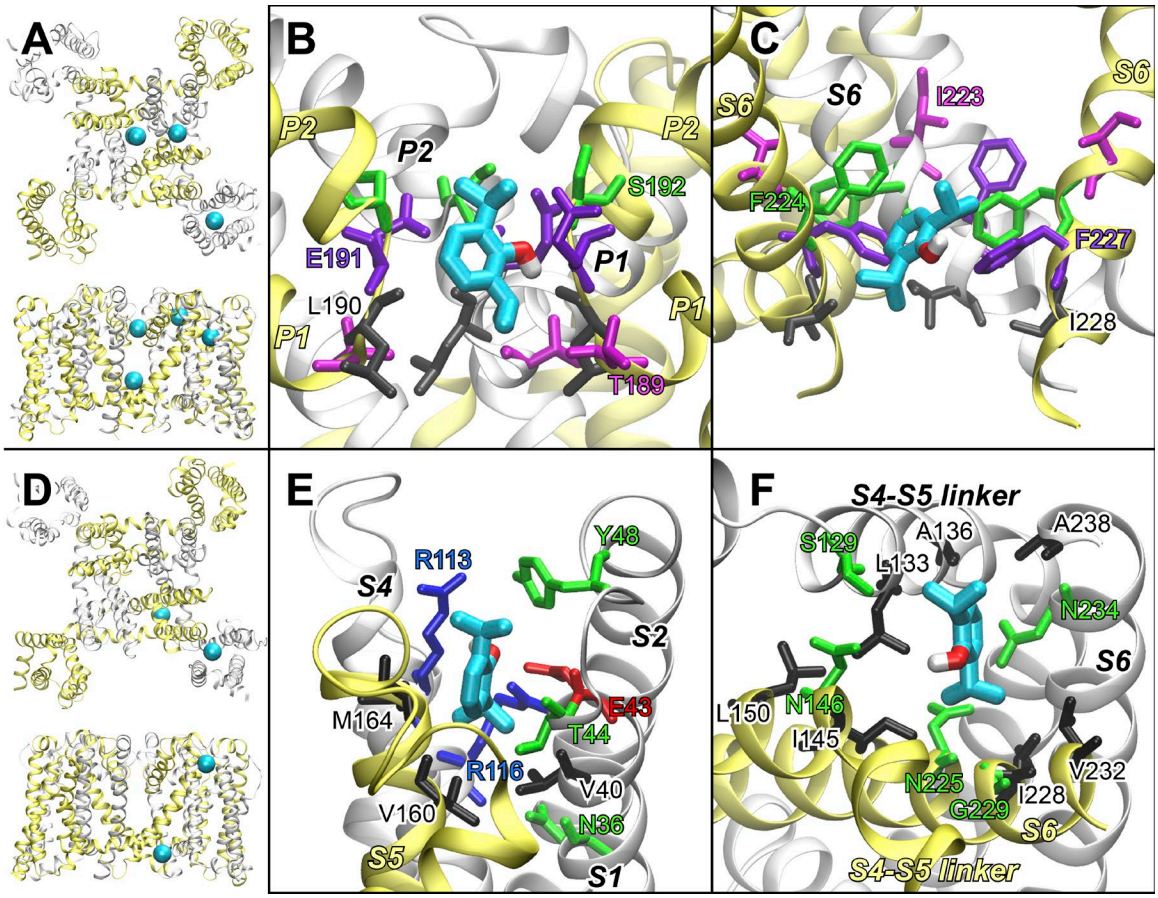

Figure 3. **In silico predicted propofol binding sites in NaChBac. (A)** Top and side views of a NaChBac structure model with putative propofol binding sites identified by molecular docking (cyan spheres, occupancy ≥ 10%). **(B and C)** Zoomed-in views of the lowest energy conformation from docking calculations of propofol (cyan) bound to NaChBac inside the pore at the selectivity filter (B) and above the activation gate (C). Residues in close proximity to the docked propofol are shown as sticks labeled with the corresponding color. Note that residues selected for ^{19}F labeling in STD NMR experiments (T189, I223, F227) are within the binding sites but unlikely to be essential for propofol binding to these regions. **(D)** Top and side views of NaChBac from the final frame of the 1-µs flooding MD simulation with putative propofol-binding sites (cyan spheres, occupancy ≥ 90%). **(E and F)** Zoomed-in views of propofol bound to NaChBac in the final frame of the 1-µs flooding MD simulation in the apex of the voltage-sensing domain (E) and an intersubunit site at the intracellular interface (F). Residues in close proximity to the docked propofol are shown as sticks labeled with the corresponding color. Note that residues selected for ^{19}F labeling in STD NMR experiments (N36, V40, S129, L150) are within the binding sites but unlikely to be essential for propofol binding to these regions.

cies and energies, analogous to the in vitro and in vivo functional results above, indicating there are no significant differences in propofol and 4-fluoropropofol binding to NaChBac. In addition, docking propofol and 4-fluoropropofol to the original (experimental) template crystal structures of Na_V channels used to construct the five NaChBac models did not reveal any additional binding sites (Table S1).

Docking results from four of the five NaChBac structures showed the highest propofol/4-fluoropropofol occupancy at the same binding site within the selectivity filter inside the pore (Fig. 3 B). One other potential binding site, inside the central pore cavity directly above the activation gate, was also observed in two of the five NaChBac structures but with lower occupancy than the selectivity filter site (Fig. 3 C). The combined docking results show a high likelihood for propofol binding at these two sites and consequently both were considered in subsequent ^{19}F STD NMR experiments. The other two potential binding sites (the apex of the VSD and an intersubunit site at the extracellular interface of the PD) were observed in the docking results from only one of the five screened NaChBac structures (Table 1); because these docking calculations provide only a rough estimate of potential propofol binding sites, an additional MD simulation of NaChBac conducted with an excess of propofol was performed to further clarify which sites have the highest potential for propofol binding.

Within the first 150 ns of the flooding simulation, nearly all propofol molecules partitioned into the lipid bilayer membrane and accumulated near the transmembrane surface of NaChBac. A propofol density map averaged over the course of the following 1-µs simulation revealed two binding sites with >90% occupancy, i.e., sites where propofol was persistently bound after the initial equilibration (Fig. 3 D). The first is a site in the apex of the VSD at the N-terminal end of the S4 helix, matching that observed previously in molecular docking on one of the screened NaChBac structures (Fig. 3 E). The second is an intersubunit site at the intracellular interface between the S4–S5 linker helix of one subunit and the S5 and S6 helices of another subunit (Fig. 3 F). With such a high occupancy throughout the simulation providing

Table 1. **Potential propofol binding sites in NaChBac identified by molecular docking**

Binding site	NaChBac template structure (PDB)	Compound[a]	Occupancy	Lowest energy score
			%	*kcal/mol*
Selectivity filter	NavAb (3RVY)	PFL	51.2	−6.20
		4FPFL	70.2	−6.19
	NavAb (5VB2)	PFL	99.6	−6.76
		4FPFL	90.6	−6.53
	NavAb (5VB8)	PFL	98.4	−6.71
		4FPFL	81.6	−6.58
	NavMs (5HVX)	PFL	100.0	−6.92
		4FPFL	98.2	−6.64
Activation gate	NavAb (5VB8)	PFL	1.6	−6.56
		4FPFL	17.6	−6.44
	NavRh (4DXW)	PFL	19.7	−6.52
		4FPFL	33.8	−6.50
Voltage sensing domain	NavAb (3RVY)	PFL	39.6	−6.61
		4FPFL	24.0	−6.72
Intersubunit extracellular interface	NavRh (4DXW)	PFL	63.5	−6.49
		4FPFL	52.5	−6.53

[a]PFL, propofol; 4FPFL, 4-fluoropropofol.

strong in silico evidence of propofol binding, these two potential sites were also considered in subsequent ^{19}F STD NMR experiments. In total, computational screening implicated four binding sites for favorable propofol binding: the selectivity filter, the activation gate in the pore, the apex of the VSD, and the S4–S5 linker.

An intrasubunit binding site at the extracellular interface of the PD, which was confirmed to bind the volatile anesthetic isoflurane (Kinde et al., 2016), was not predicted to bind propofol by either computational approach. This intrasubunit site (S208) was also included in the following ^{19}F STD NMR experiments as a measure of nonspecific propofol binding, i.e., to serve as a negative control for residual ^{19}F magnetization transfer.

Mutational analysis of putative 4-fluoropropofol binding sites

Residue-specific binding analyses with ^{19}F STD NMR require cysteine residues for selective ^{19}F labeling. Cysteine mutations are typically well tolerated in membrane proteins; however, any mutation has the potential to disrupt drug binding. Molecular details of the putative propofol binding sites predicted by the computational calculations described above were used to identify residues within the binding sites that were unlikely to be critical for propofol binding (T189, F227, V40, and S129; Fig. 3). We then investigated the effects of the introduced cysteines at each potential binding site on NaChBac channel function and 4-fluoropropofol inhibition. Fig. 4 A compares the voltage dependence of activation and inactivation for WT and the four NaChBac mutants. The gating parameters are summarized in Table 2. All four mutants exhibited baseline $V_{1/2}$ values of activation that were not statistically different from that of the WT (one-way ANOVA with Bonferroni post hoc correction), and only S129C demonstrated changes in the effective gating charge of activation. At baseline, S129C and F227C had prepulse inactivation curves that were hyperpolarized compared with the WT, whereas that of V40C was depolarized compared with the WT (Table 2). Cysteine mutations at S129 and F227 reduced the effective gating charge of inactivation and accelerated the rate of current decay (Fig. S2). However, the mutations overall were well tolerated, with some changes seen with mutations at locations critical for gating (e.g. the S4–S5 linker and activation gate).

The effects of 4 µM 4-fluoropropofol on the voltage dependence of activation and inactivation of each mutant compared with the WT are depicted in Fig. 4, B–D, and summarized in Table 3. In all mutants except F227C, 4 µM 4-fluoropropofol induced hyperpolarizing shifts in the $V_{1/2}$ values of activation compared with the respective control without 4-fluoropropofol (Fig. S3), and the $\Delta V_{1/2}$ of these shifts was not significantly different between the WT and all four mutants (one-way ANOVA with Bonferroni post hoc correction; Fig. 4 B). In addition, in all mutants except S129C, the presence of 4 µM 4-fluoropropofol also produced hyperpolarizing shifts in the $V_{1/2}$ values of inactivation compared with the respective control (Fig. S3), and the $\Delta V_{1/2}$ of these shifts was not significantly different between WT and all mutants except S129C (one-way ANOVA, Bonferroni post hoc correction). The mutant S129C showed a significantly smaller $\Delta V_{1/2}$ of inactivation by 4 µM 4-fluoropropofol than the WT (Fig. 4 C), but this is likely because the S129C mutation already strongly hyperpolarized the prepulse inactivation curve under basal conditions (Fig. S2). Similar to what we observed for propofol (Yang et al., 2018a), 4-fluoropropofol accelerated the rate of current decay (Fig. S3) and in all four mutants, the

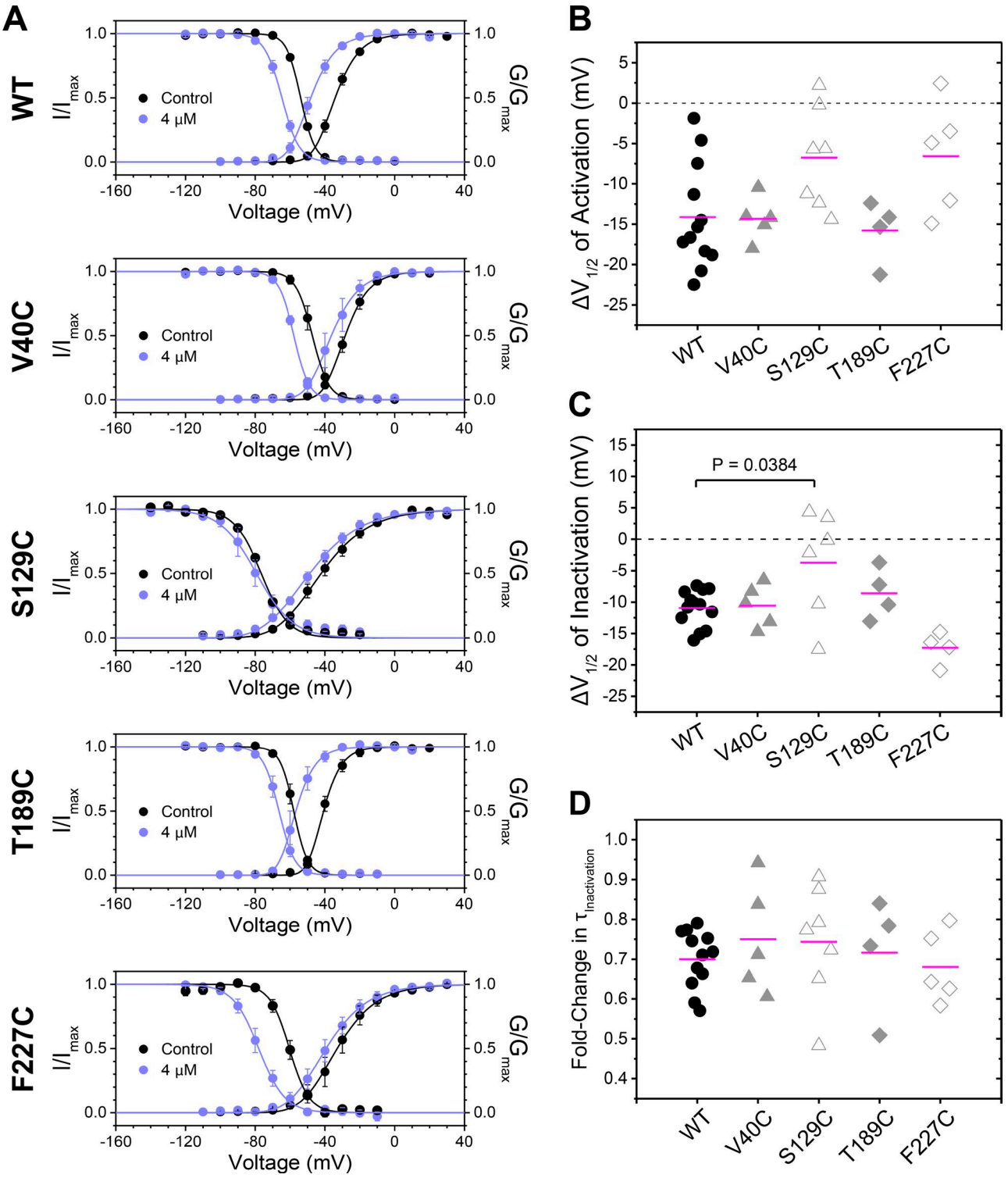

Figure 4. **Effects of single-cysteine mutations on NaChBac modulation by 4-fluoropropofol. (A)** Paired G-V and prepulse inactivation curves without (black) and with (light blue) 4 μM 4-fluoropropofol (n = 4–13) for WT and each NaChBac mutant. **(B and C)** $\Delta V_{1/2}$ values of activation (B) and inactivation (C) induced by 4 μM 4-fluoropropofol for WT and NaChBac mutants. The $\Delta V_{1/2}$ values of activation were not significantly different between WT and the mutants. Of the four mutants, only S129C shows significantly different $\Delta V_{1/2}$ of inactivation from the WT (P = 0.0384, one-way ANOVA with Bonferroni post hoc correction). **(D)** Fold-change in time constants (τ) of inactivation ($\tau_{4\text{-fluoropropofol}}/\tau_{control}$) at +20 mV induced by 4 μM 4-fluoropropofol. Time constants were derived from the decaying phase of the Na^+ currents, which were well described by the single exponential function. For all mutants, the fold-change in $\tau_{Inactivation}$ caused by 4 μM 4-fluoropropofol was not significantly different from that of WT (one-way ANOVA with Bonferroni post hoc correction). Data are reported as mean ± SEM from n independent measurements.

Table 2. **Baseline gating parameters of NaChBac single-cysteine mutants**

NaChBac mutant	Activation		Inactivation	
	$V_{1/2}$	z	$V_{1/2}$	z
	mV	e_0	*mV*	e_0
WT	−33.93 ± 1.26	3.34 ± 0.19	−54.08 ± 0.53	6.73 ± 0.28
V40C	−28.15 ± 1.62	3.29 ± 0.38	−47.34 ± 1.96***	6.19 ± 0.32
S129C	−41.68 ± 2.64	1.66 ± 0.17*	−77.84 ± 0.65***	3.66 ± 0.33*
T189C	−40.48 ± 1.09	4.23 ± 0.82	−58.04 ± 1.22	7.01 ± 0.33
F227C	−32.56 ± 4.36	2.18 ± 0.21	−60.84 ± 1.73**	5.07 ± 0.57*

Values are given as mean ± SEM (n = 4–12). Gating parameters of NaChBac WT versus each mutant, evaluated by one-way ANOVA with Bonferroni post hoc correction: *, P < 0.05; **, P < 0.01; ***, P < 0.0001.

fold-change in the time constants of inactivation induced by 4 µM 4-fluoropropofol at +20 mV was not significantly different from that in the WT (Fig. 4 D). These results provide additional evidence that the selected cysteine mutations did not hamper voltage-dependent gating or the functional responses to 4-fluoropropofol, which were generally similar to those for propofol (Yang et al., 2018a).

Residue-specific interactions quantified by ^{19}F STD NMR measurements

For each of the four potential propofol binding sites identified by computational screening (T189, F227, V40, and S129) as well as the negative control binding site at the extracellular interface of the PD (S208), single-cysteine NaChBac mutants were prepared and covalently linked to a BTFA probe to produce residue-specific ^{19}F protein resonance. Additional NaChBac mutants were similarly prepared for three of the putative binding sites for further confirmation of propofol interactions at the specific sites (I223C, N36C, and L150C). Mutations to other residues in the predicted binding site at the selectivity filter were likely to disrupt propofol binding and/or native channel function, so only T189C was considered at that site. The distance limit of detection for ^{19}F STD NMR is <10 Å (Jayalakshmi and Rama Krishna, 2002, 2004); the five regions of NaChBac examined by NMR are separated from each other by at least 15 Å. Hence, the observed STD signal is produced by 4-fluoropropofol binding close to the ^{19}F-labeled residue and does not include any long-range effects from binding to another region of NaChBac. The ^{19}F-labeling efficiency for most mutants was 20–50%, except for N36C and F227C, which had ∼10% ^{19}F labeling efficiency. Because ^{19}F-NMR background signal is nonexistent in proteins, the relatively low labeling efficiency is sufficient for STD measurements. In addition, we confirmed that unlabeled NaChBac produced STD signals for 4-fluoropropofol that were indistinguishable from noise, i.e., the on- and off-resonance spectra had equal intensities (equal I_{on} and I_{off} in Eq. 2) at the 4-fluoropropofol peak position, leading to complete cancellation of STD signals. This suggests that (a) unlabeled NaChBac (NMR invisible) does not interfere with the STD results, and (b) any imperfections in NMR hardware were below the detection limit. Note that the functional analysis of cysteine mutations described above was performed for unlabeled NaChBac mutants. Although labeling with BTFA probe might influence the function of the NaChBac mutants, this effect would be exceedingly difficult to observe: labeling efficiency in live cells is expected to be even lower than that achieved for NMR samples. Unlike ^{19}F-NMR experiments in which only the labeled proteins contribute to the STD signals, the majority of the response in electrophysiology experiments would be mostly from unlabeled protein because

Table 3. **Changes in NaChBac gating parameters induced by 4 µM 4-fluoropropofol**

NaChBac mutant	Activation		Inactivation	
	$\Delta V_{1/2}$	Δz	$\Delta V_{1/2}$	Δz
	mV	e_0	*mV*	e_0
WT	−14.11 ± 1.87§§§	0.24 ± 0.32	−10.96 ± 0.80§§§	−0.78 ± 0.21
V40C	−14.33 ± 1.20§§§	0.29 ± 0.35	−10.56 ± 1.51§§	−0.28 ± 0.32
S129C	−6.76 ± 2.37§	−0.17 ± 0.08	−3.73 ± 3.49*	0.20 ± 0.81
T189C	−15.77 ± 1.92§§	0.80 ± 0.14§	−8.61 ± 2.02§	−0.78 ± 0.26
F227C	−6.58 ± 3.11	−0.26 ± 0.18	−17.30 ± 1.29§§§	−4.80 ± 0.58§§,***

Values are given as mean ± SEM (n = 4–13). Control versus 4-fluoropropofol for each mutant, evaluated by paired t test: §, P < 0.05; §§, P < 0.01; §§§, P < 0.001. Change induced by 4-fluoropropofol in NaChBac WT versus in each mutant, evaluated by one-way ANOVA with Bonferroni post hoc correction: *, P < 0.05; ***, P < 1E-4.

of low labeling efficiency, essentially nullifying any attempts to chemically label live cells for functional measurements.

Fig. 5 A depicts representative ^{19}F-NMR spectra showing well-separated protein and 4-fluoropropofol peaks around −83.8 ppm and −121.7 ppm, respectively. Fig. 5 B is a stack plot of STD spectra showing an example of strong intermolecular saturation transfers between 4-fluoropropofol and a BTFA probe placed at S129C in the S4–S5 linker. Additional ^{19}F-NMR spectra for the other tested NaChBac mutants are shown in the online supplemental materials (Fig. S4). In contrast to S129C, saturation of the BTFA resonance linked to S208C produces very weak saturation transfer to 4-fluoropropofol (Fig. 5 C). Fig. 6 summarizes the STD accumulations as a function of saturation time for various mutants grouped by binding site. The solid lines are best fit to the data by using Eq. 1. The cross-relaxation rate constants from the fitting are summarized in Table 4. As expected, 4-fluoropropofol does not bind measurably to the intrasubunit site at the extracellular interfacial region (Fig. 6 A): although the maximum STD accumulation from S208C to 4-fluoropropofol is nonzero (3%), the curve–fit saturation time constant (k_{sat}) is not different from zero based on the Student's *t* test at the 95% significance level. In contrast, 4-fluoropropofol shows significant resonance transfer to residues in all four predicted binding sites (Fig. 6, B–D). The largest cross relaxation occurs between 4-fluoropropofol and F227C in the activation gate at the cytoplasmic entrance to the pore region. The next strongest 4-fluoropropofol cross relaxation is observed in the pocket at apex of the VSD, right above the hydrophobic constriction site at the crossing of the S4 and S1 helices (N36C, V40C). Another binding site bordered by S129C at the beginning of the S4–S5 linker and L150C in the S5 helix of the adjacent subunit also showed strong STD build-up to 4-fluoropropofol. Finally, the end of the selectivity filter (T189C) and the central cavity of the pore (I223C) also show sizable saturation transfer from the protein resonance to the 4-fluoropropofol resonance, suggesting that a significant amount of 4-fluoropropofol is likely trapped inside the pore.

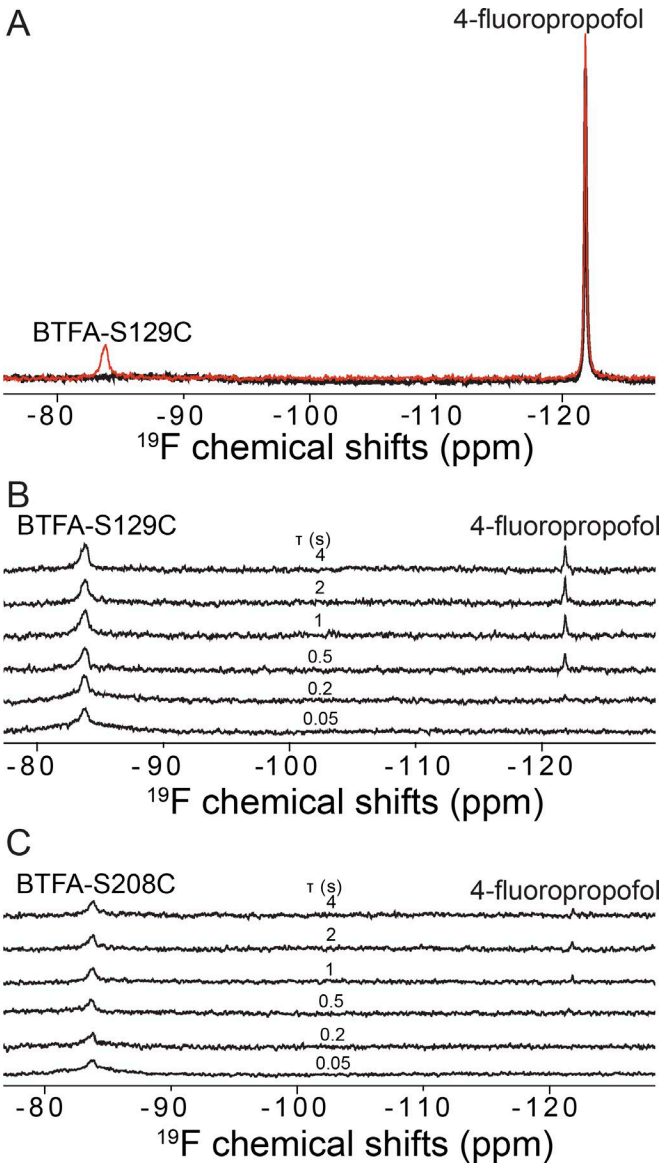

Figure 5. **^{19}F-NMR measurements of 4-fluoropropofol binding to NaChBac. (A)** Representative ^{19}F-NMR spectra of the BTFA-labeled S129C NaChBac mutant in the presence of 200 µM 4-fluoropropofol with selective on- (black, I_{on}) and off-resonance (red, I_{off}) saturation of the BTFA peak. The saturation time was 2 s. **(B)** Stack plot of ^{19}F STD NMR spectra showing that 4-fluoropropofol interacts specifically with the BTFA labeled at S129C for intermolecular saturation transfer to be built up at longer saturation time (τ). **(C)** Stack plot of ^{19}F STD NMR spectra showing that 4-fluoropropofol has no measurable interaction with the negative control BTFA-labeled S208C NaChBac.

Discussion

In this study, we combined computational prediction and site-directed intermolecular ^{19}F-NMR STD measurements to identify specific propofol-binding sites in NaChBac. At least four distinct sites have been identified by their STD cross-relaxation rates. We do not exclude the possibility that other propofol-binding sites in NaChBac may exist that were not examined in this study, including the site at the intersubunit extracellular interface (Table 1). The same intersubunit site was found in a propofol-flooding MD simulation on NavMs (Yang et al., 2018a). As mentioned in the introduction, the rate of saturation transfer depends on several factors, including dynamics of the protein and ligand, residence time of the ligand in the binding site, and orientation of the ^{19}F probes on the protein and ligand (Streiff et al., 2004; Angulo et al., 2010; Venkitakrishnan et al., 2012). As such, the cross-relaxation rate constant is a direct measure of the net magnetization transfer and hence the binding affinity between the ^{19}F labels on NaChBac and 4-fluoropropofol. It should be noted, however, that the σ values cannot be directly interpreted in terms of apparent K_d without additional measurements at other ligand concentrations. It should also be noted that the 4-fluoropropofol concentration used in the NMR experiments (200 µM) is higher than those used in the electrophysiology measurements (4 and 40 µM) because of the low NMR detection sensitivity. However, the clinical propofol concentration required to produce loss of consciousness in humans can be as high as 160 µM in the plasma (Khan et al., 2014), and the plasma concentration is typically only 1–3% of the total propofol partitioned in the lipophilic compartment of the blood and brain tissue (Sall et al., 2012).

Table 4. **Summary of 4-fluoropropofol binding at various sites in NaChBac**

Region	Residue	STD_{max}	k_{sat}	σ × 100
		%	s^{-1}	s^{-1}
Intrasubunit extracellular interface	S208	3.0 ± 1.0*	0.7 ± 0.5	2.1 ± 1.7
Voltage sensing domain	N36	11.4 ± 0.5***	2.0 ± 0.3**	22.3 ± 3.7**
	V40	9.1 ± 0.5***	2.8 ± 0.6**	25.5 ± 5.5**
S4–S5 linker	S129	8.4 ± 0.3***	1.9 ± 0.3**	15.8 ± 2.7**
	L150	9.5 ± 0.6***	1.6 ± 0.3**	15.5 ± 3.1**
Selectivity filter	T189	9.0 ± 0.5***	2.2 ± 0.4**	19.7 ± 3.8**
Activation gate	F227	17.4 ± 0.9***	2.5 ± 0.4**	42.6 ± 7.6**
	I223	9.7 ± 0.5***	1.4 ± 0.2**	13.3 ± 2.3**
	I223[a]	10.0 ± 0.4†	1.7 ± 0.2†	17.4 ± 1.5††
	I223[b]	8.0 ± 0.5†	1.1 ± 0.2†	8.4 ± 1.2††

Values are given as mean ± SEM. Difference from zero was evaluated individually for each parameter by the Student's *t* test: *, P < 0.05; **, P < 0.01; ***, P < 0.001. Difference between parameters obtained in the absence and presence of etidocaine was evaluated by the Student's *t* test: †, P < 0.05; ††, P < 0.01.
[a]Measured by using 100 µM 4-fluoropropofol without the local anesthetic etidocaine.
[b]Measured by using 100 µM 4-fluoropropofol in competition with 50 µM etidocaine.

The four propofol-binding sites identified in this study can be grouped into three separate regions. The first is in the PD within the ion-conducting passage, where propofol is found to interact with residues at the base of the selectivity filter (T189), inside the central cavity (I223), and at the activation gate (F227). The other two regions are in the apex of the VSD (N36, V40) and between the S4–S5 linker and the S5 or S6 helix from an adjacent subunit (S129, L150). At clinically relevant concentrations, one or more of these binding sites can potentially be occupied.

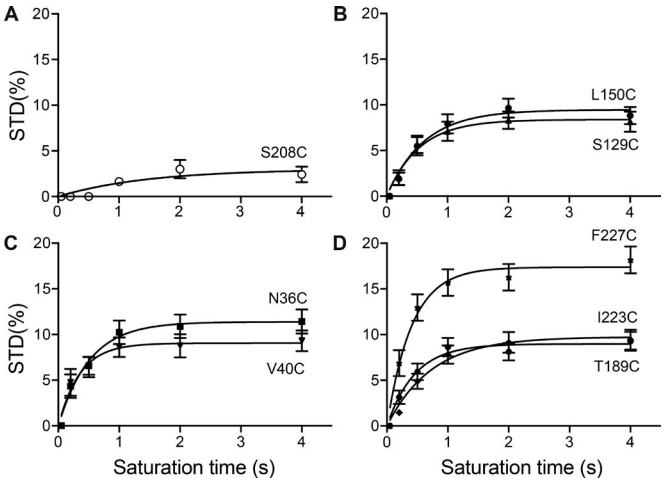

Figure 6. **Quantitative analysis of ^{19}F NMR STD build-up from individual mutation sites in NaChBac to 4-fluoropropofol.** Mutations are grouped by four regions: **(A)** the extracellular interface (S208), **(B)** the S4–S5 linker region (L150C, S129C), **(C)** the apex of the voltage sensing domain (N36C, V40C), and **(D)** the pore region (F227C, I223, T189C). The solid lines are the best fit to the data by using the two-parameter equation (Eq. 1), yielding the cross-relaxation rate constant and the saturating magnetization transfer from the ^{19}F labels on NaChBac to 4-fluoropropofol. Error bars are uncertainties calculated from the root-mean-squared noise-to-signal ratios in the on- and off-resonance ^{19}F NMR spectra.

Site-directed ^{19}F-NMR measurements strongly support the notion that multiple sites are involved in the allosteric modulation of NaChBac by propofol. It is also possible that occupancy of these sites is state dependent because all identified sites are associated with regions known to change conformation during activation and/or inactivation of voltage-gated ion channels. In particular, the aqueous cleft above the hydrophobic constriction site in the VSD and the interhelical packing between the S4–S5 linker and its interfacing S5 and S6 helices from the adjacent subunits are critical for electromechanical coupling. However, because NMR measurements were necessarily performed at depolarized (zero) cross-membrane potential, additional experiments are required to explore this possibility.

The fluorinated propofol partitioned into the channel pore and showed intermolecular ^{19}F saturation transfer with T189, the residue that marks the border between the narrow selectivity filter and the broad central aqueous cavity. An interpretation of this result is that the strong and specific interaction between 4-fluoropropofol and T189 causes drug-induced conformational changes in the selectivity filter (Pavlov et al., 2005), leading to an accelerated inactivation. An alternative interpretation supports the notion that high concentrations of propofol may partition into the pore to directly influence Na^+ conductance. However, electrophysiology data detailed in the companion paper (Yang et al., 2018a) suggest that propofol at low concentrations does not block the pore of NaChBac. Therefore, it is possible that the central cavity weakly binds propofol at all pore-lining residues from T189 down to F227. Supporting this possibility, our results with 40 µM 4-fluoropropofol (Figs. 2 and S1) showed that the predominant action of propofol at high concentrations involved pore blockade via weak interactions, as indicated by the truncation of the peak current and dramatically accelerated current decay, suggesting the possible involvement of blocking kinetics. The accelerated current decay confounds the hyperpolarizing shift in the G-V curve otherwise

observed at low propofol and 4-fluoropropofol concentrations. At 40 µM, 4-fluoropropofol also induced a dramatic hyperpolarizing shift of the prepulse inactivation curve, which additionally appeared shallower, suggesting a slower recovery from inactivation because of pore blockade-induced stabilization of the inactivated state.

The site with the largest cross-relaxation rate constant identified in the current study is located at the activation gate (F227; Fig. 6). As discussed above, the predominant action of propofol at high concentrations is to accelerate inactivation. This acceleration can be attributed, at least partially, to propofol binding near the activation gate at F227, especially considering the electrophysiology evidence that the F227C mutation by itself accelerates the rate of current decay and moves the $V_{1/2}$ of inactivation significantly in the hyperpolarization direction relative to that of the WT NaChBac (Table 2 and Fig. S2). Although the F227C mutation alone did induce a significant shift in the $\Delta Z_{inactivation}$ by 4-fluoropropofol compared with WT NaChBac (Table 3), the strong cross relaxation between fluorine probes at F227 and 4-fluoropropofol suggests that, at the concentration used in NMR studies, 4-fluoropropofol accumulates inside the pore of NaChBac. It is conceivable that occupying the site near F227 by amphipathic drugs like propofol may sensitively promote channel inactivation.

A similar mechanism of action has been proposed for local anesthetics that block the Na_V channel pore and stabilize the inactivated state (Goldschen-Ohm and Chanda, 2014): mutagenesis experiments have implicated $Na_V1.2$ residues F1764 and Y1771 (equivalent to NaChBac residues T220 and F227, respectively [Boiteux et al., 2014]) in local anesthetic binding (Ragsdale et al., 1994). To further investigate whether local anesthetics and propofol have an intersecting site of action in the pore of NaChBac, we measured the STD signal from I223C to 4-fluoropropofol in the absence and presence of 50 µM etidocaine (Fig. 7). In general, STD NMR experiments are intrinsically insensitive to silent competition partners because the STD signal is the result of an accumulation of magnetization saturation transfer from the protein to the ligand in fast exchange over a relatively long acquisition period. However, at a lower concentration of 4-fluoropropofol (100 µM), the relatively tight binding of etidocaine (K_d ~1 µM for the inactivated state of $Na_V1.2$ [Ragsdale et al., 1994]) allowed us to observe a significant decrease in the cross-relaxation rate of 4-fluoropropofol binding in the pore of NaChBac (Table 4). Thus, although the mechanisms may differ, local anesthetics and propofol seem to share an overlapping site of action. Additional ^{19}F STD NMR experiments with a fluorinated local anesthetic analogue or electrophysiological competition experiments could be used to further support this prediction.

Binding to the apex of the VSD has not been reported before for any general anesthetic but is supported here by direct experimental measures of intermolecular ^{19}F saturation transfer. Anesthetic binding at this site likely modulates gating charge movement. A previous study suggested that the sliding of gating charges across a hydrophobic "girdle" depends on favorable electrostatic interactions of the gating charges against the complementary surfaces that consist of an extracellular negative-charge cluster and intracellular negative-charge cluster (Payandeh et al., 2011). The major energy barrier comes from moving the gating charges in the S4 helix to pass a focused electric field at the hydrophobic constriction site. It is conceivable that amphipathic propofol or 4-fluoropropofol molecules located between the hydrophobic girdle and the hydrophilic water molecules in the aqueous cleft facilitate the sliding movement of S4, favoring a transition to the open state. This is consistent with the parallel leftward shift of the G-V curve observed in this study with 4-fluoropropofol and in our other studies with propofol (Yang et al., 2018a). However, it is import-

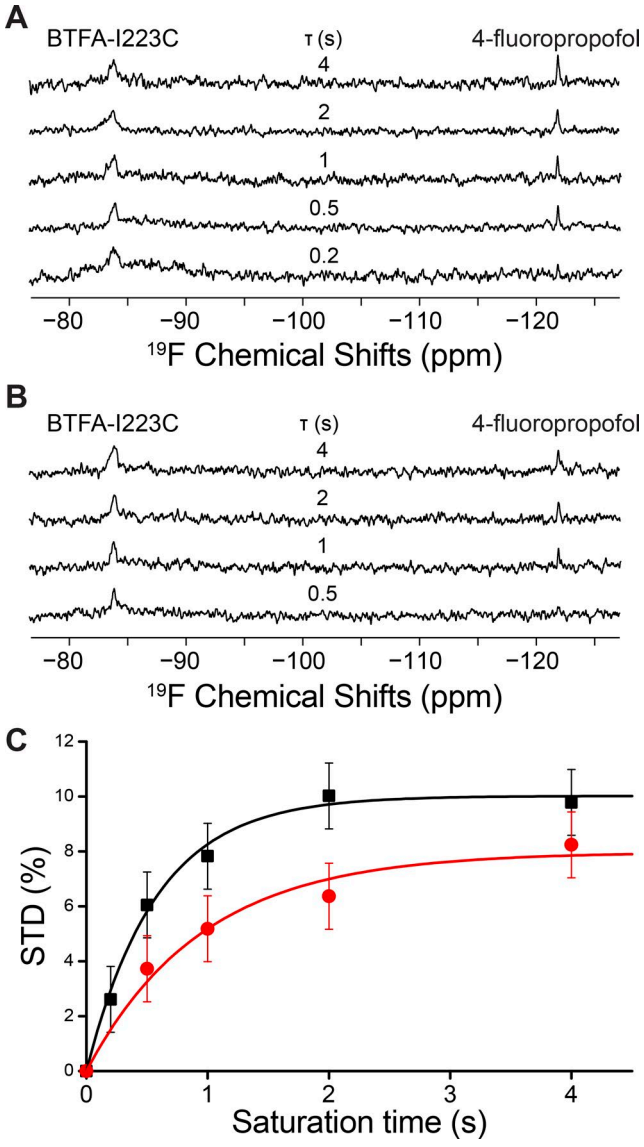

Figure 7. **Local anesthetic inhibition of 4-fluoropropofol ^{19}F NMR STD signal in the pore of NaChBac. (A and B)** Stack plots of ^{19}F STD NMR spectra for 100 µM 4-fluoropropofol interacting with the BTFA labeled at I223C in the absence (A) and presence (B) of 50 µM etidocaine, a local anesthetic. **(C)** ^{19}F NMR STD accumulation in the absence (black) and presence (red) of 50 µM etidocaine. The solid lines are the best fit to the data by using the two-parameter equation (Eq. 1), yielding the cross-relaxation rate constant and the saturating magnetization transfer from the ^{19}F labels on I223C in NaChBac to 4-fluoropropofol. Error bars are uncertainties calculated from the root-mean-square noise-to-signal ratios in the on- and off-resonance ^{19}F NMR spectra.

ant to note that as the NMR measurements were performed at depolarized (zero) cross-membrane potential, it is also possible that the 4-fluoropropofol binding at the apex of VSD is state-dependent and favors activated states (open and inactivated) over the resting states.

Like the volatile anesthetic isoflurane, 4-fluoropropofol interacts specifically with the ^{19}F labels placed at S129C and L150C, which in our structure model of NaChBac form a well-defined intersubunit pocket at the intracellular interface. However, the contributions of propofol binding at this site to channel function are complicated by the fact that the S129C mutation alone induced hyperpolarizing shifts in the voltage-dependence of activation and inactivation and accelerated the rate of channel inactivation (Table 2 and Fig. S2). Although our ^{19}F STD measurements provide direct experimental evidence showing the involvement of the S4–S5 linker in propofol binding, how the binding at this site facilitates channel activation or accelerates slow inactivation, or both, requires further investigations. A possible scenario, based on the novel role of S4–S5 linker in the inactivation of eukaryotic Na_V subchannels, is proposed in the companion paper (Yang et al., 2018a).

Conclusion

Direct experimental evidence from this study supports the notion that the intravenous general anesthetic propofol binds to multiple sites in the prokaryotic Na_V channel NaChBac for allosteric modulation of gating. Propofol produces a net effect of inhibition to channel function by facilitating the activation process and potently promoting the slow inactivation process, shifting the channel population from the resting to the inactivated states. Based on the locations of the propofol binding sites identified in this study, we hypothesize that propofol binding in the apex of VSD above the hydrophobic constriction site facilitates channel activation, whereas the binding in the channel pore, particularly at the activation gate near F227, accelerates channel inactivation. Propofol binding near the S4–S5 linker site might play a dual role by promoting opening and entry into an inactivated state. Additional experiments, however, are required to confirm these hypotheses.

Acknowledgments

We thank Sandy Hirsch for editorial assistance.

This work was supported in part by grants from the National Institutes of Health (R01GM056257, R01GM049202, P01GM055876, and F30GM123612).

The authors declare no competing financial interests.

Author contributions: P. Tang and Y. Xu designed the study. Y. Wang and V. Bondarenko expressed and purified proteins, carried out NMR experiments, and analyzed data. E. Yang performed electrophysiology measurements and analyzed data. M.M. Wells, V. Carnevale, and D. Granata performed computational modeling, docking, and MD simulations. K. Woll performed in vivo tadpole experiments. W.P. Dailey synthesized 4-fluoropropofol. M.L. Klein, R.G. Eckenhoff, M. Covarrubias, P. Tang, and Y. Xu secured funding for the project. Y. Xu, P. Tang, and M. Covarrubias analyzed and interpreted data. Y. Xu and M.M. Wells wrote the paper with input from the other coauthors.

Kenton J. Swartz served as editor.

Submitted: 6 January 2018
Revised: 2 May 2018
Accepted: 15 June 2018

References

Amarouch, M.Y., and H. Abriel. 2015. Cellular hyper-excitability caused by mutations that alter the activation process of voltage-gated sodium channels. *Front. Physiol.* 6:45. https://doi.org/10.3389/fphys.2015.00045

Angulo, J., P.M. Enríquez-Navas, and P.M. Nieto. 2010. Ligand-receptor binding affinities from saturation transfer difference (STD) NMR spectroscopy: the binding isotherm of STD initial growth rates. *Chemistry.* 16:7803–7812. https://doi.org/10.1002/chem.200903528

Barber, A.F., V. Carnevale, S.G. Raju, C. Amaral, W. Treptow, and M.L. Klein. 2012. Hinge-bending motions in the pore domain of a bacterial voltage-gated sodium channel. *Biochim. Biophys. Acta.* 1818:2120–2125. https://doi.org/10.1016/j.bbamem.2012.05.002

Barber, A.F., V. Carnevale, M.L. Klein, R.G. Eckenhoff, and M. Covarrubias. 2014. Modulation of a voltage-gated Na+ channel by sevoflurane involves multiple sites and distinct mechanisms. *Proc. Natl. Acad. Sci. USA.* 111:6726–6731. https://doi.org/10.1073/pnas.1405768111

Boiteux, C., I. Vorobyov, R.J. French, C. French, V. Yarov-Yarovoy, and T.W. Allen. 2014. Local anesthetic and antiepileptic drug access and binding to a bacterial voltage-gated sodium channel. *Proc. Natl. Acad. Sci. USA.* 111:13057–13062. https://doi.org/10.1073/pnas.1408710111

Bondarenko, V., D.D. Mowrey, T.S. Tillman, E. Seyoum, Y. Xu, and P. Tang. 2014. NMR structures of the human α7 nAChR transmembrane domain and associated anesthetic binding sites. *Biochim. Biophys. Acta.* 1838:1389–1395. https://doi.org/10.1016/j.bbamem.2013.12.018

Carnevale, V., W. Treptow, and M.L. Klein. 2011. Sodium ion binding sites and hydration in the lumen of a bacterial ion channel from molecular dynamics simulations. *J. Phys. Chem. Lett.* 2:2504–2508. https://doi.org/10.1021/jz2011379

Chan, H.H., M.K. Tse, S. Kumar, and L. Zhuo. 2018. A novel selective MAO-B inhibitor with neuroprotective and anti-Parkinsonian properties. *Eur. J. Pharmacol.* 818:254–262. https://doi.org/10.1016/j.ejphar.2017.10.023

Chen, Q., M.H. Cheng, Y. Xu, and P. Tang. 2010. Anesthetic binding in a pentameric ligand-gated ion channel: GLIC. *Biophys. J.* 99:1801–1809. https://doi.org/10.1016/j.bpj.2010.07.023

Danielson, M.A., and J.J. Falke. 1996. Use of 19F NMR to probe protein structure and conformational changes. *Annu. Rev. Biophys. Biomol. Struct.* 25:163–195. https://doi.org/10.1146/annurev.bb.25.060196.001115

Eckenhoff, R.G., and J.S. Johansson. 1997. Molecular interactions between inhaled anesthetics and proteins. *Pharmacol. Rev.* 49:343–367.

Frenkel, C., and B.W. Urban. 1991. Human brain sodium channels as one of the molecular target sites for the new intravenous anaesthetic propofol (2,6-diisopropylphenol). *Eur. J. Pharmacol.* 208:75–79. https://doi.org/10.1016/0922-4106(91)90054-L

Goldschen-Ohm, M.P., and B. Chanda. 2014. Probing gating mechanisms of sodium channels using pore blockers. *Handb. Exp. Pharmacol.* 221:183–201. https://doi.org/10.1007/978-3-642-41588-3_9

Habib, A.M., J.N. Wood, and J.J. Cox. 2015. Sodium channels and pain. *Handb. Exp. Pharmacol.* 227:39–56. https://doi.org/10.1007/978-3-662-46450-2_3

Haeseler, G., and M. Leuwer. 2003. High-affinity block of voltage-operated rat IIA neuronal sodium channels by 2,6 di-tert-butylphenol, a propofol analogue. *Eur. J. Anaesthesiol.* 20:220–224. https://doi.org/10.1097/00003643-200303000-00007

Haeseler, G., M. Karst, N. Foadi, S. Gudehus, A. Roeder, H. Hecker, R. Dengler, and M. Leuwer. 2008. High-affinity blockade of voltage-operated skeletal muscle and neuronal sodium channels by halogenated propofol analogues. *Br. J. Pharmacol.* 155:265–275. https://doi.org/10.1038/bjp.2008.255

Hall, M.A., J. Xi, C. Lor, S. Dai, R. Pearce, W.P. Dailey, and R.G. Eckenhoff. 2010. m-Azipropofol (AziPm) a photoactive analogue of the intravenous gen-

eral anesthetic propofol. *J. Med. Chem.* 53:5667–5675. https://doi.org/10.1021/jm1004072

Hemmings, H.C. Jr., M.H. Akabas, P.A. Goldstein, J.R. Trudell, B.A. Orser, and N.L. Harrison. 2005. Emerging molecular mechanisms of general anesthetic action. *Trends Pharmacol. Sci.* 26:503–510. https://doi.org/10.1016/j.tips.2005.08.006

Hénin, J., W. Shinoda, and M.L. Klein. 2008. United-atom acyl chains for CHARMM phospholipids. *J. Phys. Chem. B.* 112:7008–7015. https://doi.org/10.1021/jp800687p

Jayalakshmi, V., and N. Rama Krishna. 2002. Complete relaxation and conformational exchange matrix (CORCEMA) analysis of intermolecular saturation transfer effects in reversibly forming ligand-receptor complexes. *J. Magn. Reson.* 155:106–118. https://doi.org/10.1006/jmre.2001.2499

Jayalakshmi, V., and N. Rama Krishna. 2004. CORCEMA refinement of the bound ligand conformation within the protein binding pocket in reversibly forming weak complexes using STD-NMR intensities. *J. Magn. Reson.* 168:36–45. https://doi.org/10.1016/j.jmr.2004.01.017

Jeevaratnam, K., L. Guzadhur, Y.M. Goh, A.A. Grace, and C.L. Huang. 2016. Sodium channel haploinsufficiency and structural change in ventricular arrhythmogenesis. *Acta Physiol. (Oxf.).* 216:186–202. https://doi.org/10.1111/apha.12577

Khan, M.S., E.L. Zetterlund, H. Gréen, A. Oscarsson, A.L. Zackrisson, E. Svanborg, M.L. Lindholm, H. Persson, and C. Eintrei. 2014. Pharmacogenetics, plasma concentrations, clinical signs and EEG during propofol treatment. *Basic Clin. Pharmacol. Toxicol.* 115:565–570. https://doi.org/10.1111/bcpt.12277

Kinde, M.N., V. Bondarenko, D. Granata, W. Bu, K.C. Grasty, P.J. Loll, V. Carnevale, M.L. Klein, R.G. Eckenhoff, P. Tang, and Y. Xu. 2016. Fluorine-19 NMR and computational quantification of isoflurane binding to the voltage-gated sodium channel NaChBac. *Proc. Natl. Acad. Sci. USA.* 113:13762–13767. https://doi.org/10.1073/pnas.1609939113

Künze, G., J.P. Gehrcke, M.T. Pisabarro, and D. Huster. 2014. NMR characterization of the binding properties and conformation of glycosaminoglycans interacting with interleukin-10. *Glycobiology.* 24:1036–1049. https://doi.org/10.1093/glycob/cwu069

Künze, G., S. Köhling, A. Vogel, J. Rademann, and D. Huster. 2016. Identification of the glycosaminoglycan binding site of interleukin-10 by NMR spectroscopy. *J. Biol. Chem.* 291:3100–3113. https://doi.org/10.1074/jbc.M115.681759

LeBard, D.N., J. Hénin, R.G. Eckenhoff, M.L. Klein, and G. Brannigan. 2012. General anesthetics predicted to block the GLIC pore with micromolar affinity. *PLOS Comput. Biol.* 8:e1002532. https://doi.org/10.1371/journal.pcbi.1002532

Lee, J., X. Cheng, J.M. Swails, M.S. Yeom, P.K. Eastman, J.A. Lemkul, S. Wei, J. Buckner, J.C. Jeong, Y. Qi, et al. 2016. CHARMM-GUI input generator for NAMD, GROMACS, AMBER, OpenMM, and CHARMM/OpenMM simulations using the CHARMM36 additive force field. *J. Chem. Theory Comput.* 12:405–413. https://doi.org/10.1021/acs.jctc.5b00935

Lenaeus, M.J., T.M. Gamal El-Din, C. Ing, K. Ramanadane, R. Pomès, N. Zheng, and W.A. Catterall. 2017. Structures of closed and open states of a voltage-gated sodium channel. *Proc. Natl. Acad. Sci. USA.* 114:E3051–E3060. https://doi.org/10.1073/pnas.1700761114

Lepre, C.A., J.M. Moore, and J.W. Peng. 2004. Theory and applications of NMR-based screening in pharmaceutical research. *Chem. Rev.* 104:3641–3676. https://doi.org/10.1021/cr030409h

Lin, W.H., and R.A. Baines. 2015. Regulation of membrane excitability: A convergence on voltage-gated sodium conductance. *Mol. Neurobiol.* 51:57–67. https://doi.org/10.1007/s12035-014-8674-0

Liu, L.T., D. Willenbring, Y. Xu, and P. Tang. 2009. General anesthetic binding to neuronal alpha4beta2 nicotinic acetylcholine receptor and its effects on global dynamics. *J. Phys. Chem. B.* 113:12581–12589. https://doi.org/10.1021/jp9039513

Mayer, M., and B. Meyer. 1999. Characterization of ligand binding by saturation transfer difference NMR spectroscopy. *Angew. Chem. Int. Ed. Engl.* 38:1784–1788. https://doi.org/10.1002/(SICI)1521-3773(19990614)38:12%3C1784::AID-ANIE1784%3E3.0.CO;2-Q

Morris, G.M., R. Huey, W. Lindstrom, M.F. Sanner, R.K. Belew, D.S. Goodsell, and A.J. Olson. 2009. AutoDock4 and AutoDockTools4: Automated docking with selective receptor flexibility. *J. Comput. Chem.* 30:2785–2791. https://doi.org/10.1002/jcc.21256

Mowrey, D.D., Q. Liu, V. Bondarenko, Q. Chen, E. Seyoum, Y. Xu, J. Wu, and P. Tang. 2013. Insights into distinct modulation of α7 and α7β2 nicotinic acetylcholine receptors by the volatile anesthetic isoflurane. *J. Biol. Chem.* 288:35793–35800. https://doi.org/10.1074/jbc.M113.508333

OuYang, W., and H.C. Hemmings Jr. 2007. Isoform-selective effects of isoflurane on voltage-gated Na+ channels. *Anesthesiology.* 107:91–98. https://doi.org/10.1097/01.anes.0000268390.28362.4a

Ouyang, W., G. Wang, and H.C. Hemmings Jr. 2003. Isoflurane and propofol inhibit voltage-gated sodium channels in isolated rat neurohypophysial nerve terminals. *Mol. Pharmacol.* 64:373–381. https://doi.org/10.1124/mol.64.2.373

Pan, J., Q. Chen, D. Willenbring, D. Mowrey, X.P. Kong, A. Cohen, C.B. Divito, Y. Xu, and P. Tang. 2012. Structure of the pentameric ligand-gated ion channel GLIC bound with anesthetic ketamine. *Structure.* 20:1463–1469. https://doi.org/10.1016/j.str.2012.08.009

Pavlov, E., C. Bladen, R. Winkfein, C. Diao, P. Dhaliwal, and R.J. French. 2005. The pore, not cytoplasmic domains, underlies inactivation in a prokaryotic sodium channel. *Biophys. J.* 89:232–242. https://doi.org/10.1529/biophysj.104.056994

Payandeh, J., T. Scheuer, N. Zheng, and W.A. Catterall. 2011. The crystal structure of a voltage-gated sodium channel. *Nature.* 475:353–358. https://doi.org/10.1038/nature10238

Phillips, J.C., R. Braun, W. Wang, J. Gumbart, E. Tajkhorshid, E. Villa, C. Chipot, R.D. Skeel, L. Kalé, and K. Schulten. 2005. Scalable molecular dynamics with NAMD. *J. Comput. Chem.* 26:1781–1802. https://doi.org/10.1002/jcc.20289

Purtell, K., K.J. Gingrich, W. Ouyang, K.F. Herold, and H.C. Hemmings Jr. 2015. Activity-dependent depression of neuronal sodium channels by the general anaesthetic isoflurane. *Br. J. Anaesth.* 115:112–121. https://doi.org/10.1093/bja/aev203

Ragsdale, D.S., J.C. McPhee, T. Scheuer, and W.A. Catterall. 1994. Molecular determinants of state-dependent block of Na+ channels by local anesthetics. *Science.* 265:1724–1728. https://doi.org/10.1126/science.8085162

Rehberg, B., and D.S. Duch. 1999. Suppression of central nervous system sodium channels by propofol. *Anesthesiology.* 91:512–520. https://doi.org/10.1097/00000542-199908000-00026

Ren, D., B. Navarro, H. Xu, L. Yue, Q. Shi, and D.E. Clapham. 2001. A prokaryotic voltage-gated sodium channel. *Science.* 294:2372–2375. https://doi.org/10.1126/science.1065635

Sall, J.W., G. Stratmann, J. Leong, E. Woodward, and P.E. Bickler. 2012. Propofol at clinically relevant concentrations increases neuronal differentiation but is not toxic to hippocampal neural precursor cells in vitro. *Anesthesiology.* 117:1080–1090. https://doi.org/10.1097/ALN.0b013e31826f8d86

Sand, R.M., K.J. Gingrich, T. Macharadze, K.F. Herold, and H.C. Hemmings Jr. 2017. Isoflurane modulates activation and inactivation gating of the prokaryotic Na^+ channel NaChBac. *J. Gen. Physiol.* 149:623–638. https://doi.org/10.1085/jgp.201611600

Stoetzer, C., S. Reuter, T. Doll, N. Foadi, F. Wegner, and A. Leffler. 2016. Inhibition of the cardiac Na^+ channel α-subunit Nav1.5 by propofol and dexmedetomidine. *Naunyn Schmiedebergs Arch. Pharmacol.* 389:315–325. https://doi.org/10.1007/s00210-015-1195-1

Streiff, J.H., N.O. Juranic, S.I. Macura, D.O. Warner, K.A. Jones, and W.J. Perkins. 2004. Saturation transfer difference nuclear magnetic resonance spectroscopy as a method for screening proteins for anesthetic binding. *Mol. Pharmacol.* 66:929–935.

Sula, A., J. Booker, L.C. Ng, C.E. Naylor, P.G. DeCaen, and B.A. Wallace. 2017. The complete structure of an activated open sodium channel. *Nat. Commun.* 8:14205. https://doi.org/10.1038/ncomms14205

Tang, P., and Y. Xu. 2002. Large-scale molecular dynamics simulations of general anesthetic effects on the ion channel in the fully hydrated membrane: The implication of molecular mechanisms of general anesthesia. *Proc. Natl. Acad. Sci. USA.* 99:16035–16040. https://doi.org/10.1073/pnas.252522299

Tillman, T., M.H. Cheng, Q. Chen, P. Tang, and Y. Xu. 2013. Reversal of ion-charge selectivity renders the pentameric ligand-gated ion channel GLIC insensitive to anaesthetics. *Biochem. J.* 449:61–68. https://doi.org/10.1042/BJ20121072

Venkitakrishnan, R.P., O. Benard, M. Max, J.L. Markley, and F.M. Assadi-Porter. 2012. Use of NMR saturation transfer difference spectroscopy to study ligand binding to membrane proteins. *Methods Mol. Biol.* 914:47–63.

Wagstaff, J.L., S.L. Taylor, and M.J. Howard. 2013. Recent developments and applications of saturation transfer difference nuclear magnetic resonance (STD NMR) spectroscopy. *Mol. Biosyst.* 9:571–577. https://doi.org/10.1039/C2MB25395J

Webb, B., and A. Sali. 2014a. Comparative protein structure modeling using MODELLER. Curr. Protoc. Bioinformatics. 47:5.6.1–5.6.32.

Webb, B., and A. Sali. 2014b. Protein structure modeling with MODELLER. *Methods Mol. Biol.* 1137:1–15. https://doi.org/10.1007/978-1-4939-0366-5_1

Woll, K.A., B.P. Weiser, Q. Liang, T. Meng, A. McKinstry-Wu, B. Pinch, W.P. Dailey, W.D. Gao, M. Covarrubias, and R.G. Eckenhoff. 2015. Role for the propofol hydroxyl in anesthetic protein target molecular recognition. *ACS Chem. Neurosci.* 6:927–935. https://doi.org/10.1021/acschemneuro.5b00078

Yang, E., D. Granata, R.G. Eckenhoff, V. Carnevale, and M. Covarrubias. 2018a. Propofol inihibits prokaryotic voltage-gated Na^+ channels by promoting activation-coupled inactivation. *J. Gen. Physiol.* https://doi.org/10.1085/jgp.201711924

Yang, E., L. Zhi, Q. Liang, and M. Covarrubias. 2018b. Electrophysiological analysis of voltage-gated ion channel modulation by general anesthetics. *Methods Enzymol.* 602:339–368. https://doi.org/10.1016/bs.mie.2018.01.013

Yuan, D., H. Chen, D. Chen, X. Zhao, Y. Li, J. Yan, and Y. Zou. 2017. A method for preparing 2,6-diisopropyl-4-fluorophenol. Google China patent CN103896743B, filed July 2, 2014, and issued April 5, 2017.

Zhang, X., W. Ren, P. DeCaen, C. Yan, X. Tao, L. Tang, J. Wang, K. Hasegawa, T. Kumasaka, J. He, et al. 2012. Crystal structure of an orthologue of the NaChBac voltage-gated sodium channel. *Nature.* 486:130–134. https://doi.org/10.1038/nature11054

Zhang, Y.Z., H. Xu, A.M. Parsons, and L.B. Casabianca. 2017. Examining binding to nanoparticle surfaces using saturation transfer difference (STD)-NMR spectroscopy. *J. Phys. Chem. C.* 121:24678–24686. https://doi.org/10.1021/acs.jpcc.7b08828